

Visual Estimation of Fingertip Pressure on Diverse Surfaces using Easily Captured Data

Patrick Grady¹, Jeremy A. Collins¹, Chengcheng Tang², Christopher D. Twigg²,
James Hays¹, Charles C. Kemp¹

¹Georgia Institute of Technology, ²Meta Reality Labs

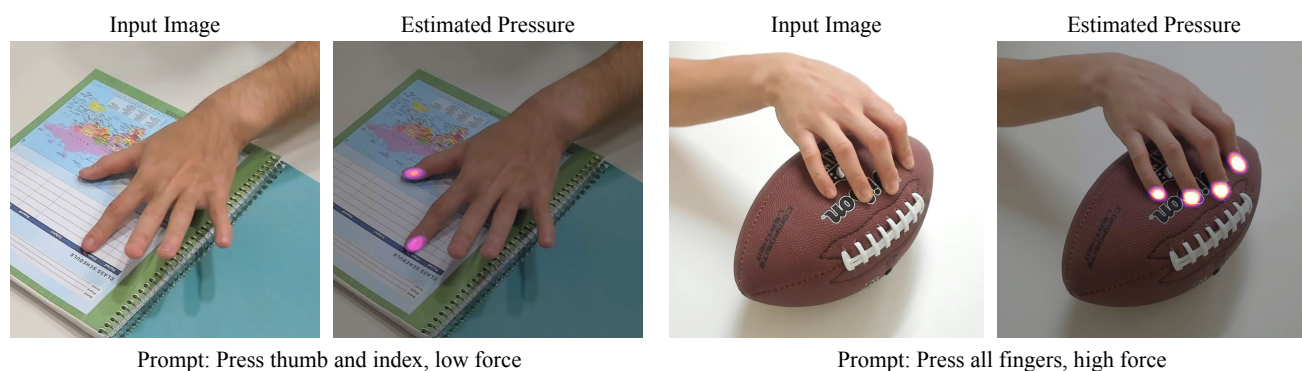


Figure 1. By leveraging *contact labels*, ContactLabelNet estimates fingertip pressure when participants interact with diverse surfaces, including highly textured (left) and curved surfaces (right).

Abstract

Prior research has shown that deep models can estimate the pressure applied by a hand to a surface based on a single RGB image. Training these models requires high-resolution pressure measurements that are difficult to obtain with physical sensors. Additionally, even experts cannot reliably annotate pressure from images. Thus, data collection is a critical barrier to generalization and improved performance. We present a novel approach that enables training data to be efficiently captured from unmodified surfaces with only an RGB camera and a cooperative participant. Our key insight is that people can be prompted to perform actions that correspond with categorical labels (contact labels) describing contact pressure, such as using a specific fingertip to make low-force contact. We present ContactLabelNet, which visually estimates pressure applied by fingertips. With the use of contact labels, ContactLabelNet achieves improved performance, generalizes to novel surfaces, and outperforms models from prior work.

1. Introduction

People frequently interact with their surroundings by applying pressure with their hands. Machine perception of

hand contact pressure has been used for activity recognition [51], ergonomics [45], user interfaces [48], and other applications. Most approaches use physical pressure sensing arrays, which can be expensive and difficult to mount.

PressureVision [17] showed that computer vision can be used to estimate hand pressure, which could enable new applications, such as touch interfaces for augmented reality. Their deep model, PressureVisionNet, estimates hand pressure from a single RGB image. The model performs well with diverse hands, but was only trained on two simple, flat, rigid surfaces, and was evaluated on the same surfaces.

Collecting training data for diverse surfaces might enable PressureVisionNet to perform well on varied surfaces, but data collection is challenging. Each RGB image in the training data requires ground truth from a high-resolution pressure sensing array registered with a camera. This requirement severely limits data collection for diverse surfaces, since mounting a high-resolution pressure sensing array alters the appearance of the surface and the surface’s mechanical properties.

We present a novel approach that enables training data for visual hand pressure estimation to be captured for unaltered surfaces found in the wild. Instead of instrumenting the surface, our approach relies on people’s highly sensitive perception of touch and manual dexterity [26]. We prompt

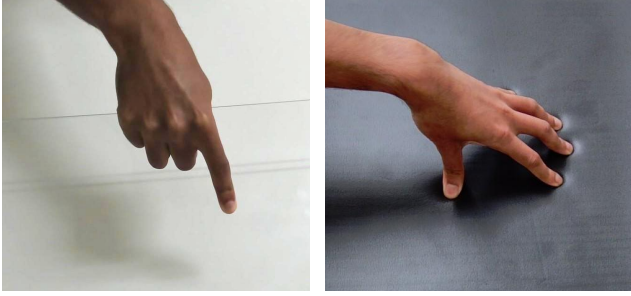


Figure 2. Instrumenting surfaces with pressure sensors without altering their properties is challenging. For example, pressure sensors must be transparent in order to instrument glass, or must be stretchable in order to instrument a deformable mat.

participants to make contact with a surface in a specific way. This prompt serves as a categorical label, which we refer to as a *contact label*. A contact label consists of the regions of the hand that are in contact with a surface and the level of applied force.

A contact label is a form of weak label [41] for an RGB image. For this paper, we use contact labels that define which fingertips are in contact and whether low or high force is being applied. We present ContactLabelNet, which estimates fingertip pressure on diverse surfaces, including surfaces with compliance, curvature, and complex textures. Training ContactLabelNet on RGB images paired with contact labels results in higher performance on diverse surfaces, outperforming prior work and generalizing to surfaces that are not represented in fully labeled training data.

In summary, we make the following contributions:

- **Pressure estimation for diverse surfaces:** We demonstrate visual estimation of pressure applied by multiple fingertips on diverse surfaces, including highly-textured, curved, and compliant surfaces.
- **Data collection using contact labels:** We present a method suitable for collecting hand pressure data in the wild which involves prompting participants to make contact that adheres to a categorical label.
- **Deep model that benefits from contact labels:** We present a deep model (ContactLabelNet) that achieves significantly higher performance when trained on RGB images with contact labels.
- **Open materials:** We will release all trained models, data, and code associated with this paper.

2. Related Work

Our research relates to approaches that sense hand pressure, especially methods using computer vision. Our deep model, ContactLabelNet, uses methods inspired by research

on unsupervised domain adaptation and learning from weak labels.

Hand-Mounted Sensors: Hands are highly articulated and have compliant surfaces that make mounting pressure sensors difficult. Human factors also present challenges since mounting sensors can decrease comfort, interfere with tactile perception, and impact manual dexterity. Glove-based sensors have been developed by researchers [9, 51] and are commercially available [44, 52]. However, the gloves occlude the surface of the hand, which interferes with data collection for visual models intended for bare hands.

Environment-Mounted Sensors: Pressure sensors can be mounted on surfaces in the environment to sense hand pressure, including capacitive sensors [2, 13, 19], force-sensitive resistors [8, 40, 43], flexible sensors [4, 28, 52], and fabric-based sensors [36]. Sensors suitable for mounting on an in-the-wild surface tend to be custom or expensive. More importantly, mounting pressure sensors alters the visual appearance and mechanical properties of the surface, which interferes with data collection for diverse in-the-wild surfaces. To objectively assess the performance contact labels, in our study we mount textured overlays on a commercially produced pressure sensing array [40]. While useful, these surfaces lack compliance, curvature, and other properties associated with in-the-wild surfaces.

Unconventional Imaging: Researchers have demonstrated methods that can detect where contact has occurred between a hand and an unmodified surface. Thermal imaging [6, 7] and laser speckle imaging [49] have been used to detect where hands have touched surfaces. These methods require additional instrumentation, do not directly report pressure, and retrospectively report where contact occurred. They can also be sensitive to surface details, such as thermal properties and specularities. In contrast to these methods, our approach only requires an inexpensive off-the-shelf RGB camera and a surface that can be safely touched in accordance with the contact label, making our method suitable for crowd-sourcing and efficient in-the-wild data collection.

Visual Hand Pressure Estimation: The force applied by a hand to a known object can be estimated by observing the object’s pose over time and finding the net force that would result in the object’s observed motion. If contact points are known, per-contact normal force can be estimated. Contact points can be estimated using neural networks [15, 31] or by combining markerless tracking of the hands with mesh-object intersection [42, 43, 47]. These methods can infer

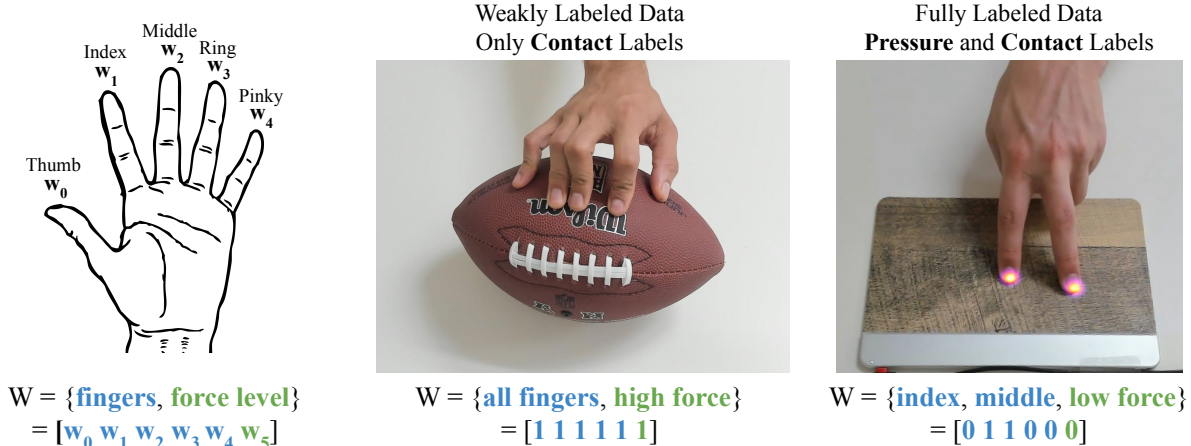


Figure 3. We represent the contact labels as a six-dimensional vector. The first five elements are binary values indicating which fingers are prompted to be in contact, and the last element indicates the prompted force level: low (0), high (1), or unspecified (-1). Fully labeled data has *both* pressure and contact labels, while weakly labeled data has *only* contact labels. [46]

contact that is occluded or out-of-view, but estimating net force based on an object requires that the object move, and thus fails for objects fixed to the environment like tabletops. Contact estimates based on mesh geometry are also sensitive to precision since contact depends on millimeter scale displacements [18].

A number of approaches have demonstrated that visual cues can be used to estimate hand pressure, including fingertip color changes [12, 37, 38], soft tissue deformation [25], and cast shadows [21, 22, 24]. In contrast to this prior work, our method uses an external camera to view the whole hand from a distance and deep learning to take advantage of multiple types of cues. As we describe elsewhere, our method builds on PressureVision [17].

Deep Learning without Labels: Unsupervised domain adaptation addresses cases when an abundance of labeled data is available in a source domain, yet no labeled data is available in a target domain. To bridge this gap, a common technique is to learn domain-invariant features by minimizing some measure of distance between source and target feature distributions [33, 53]. This can also be done by adversarially training a discriminator to classify the domain of the features [16] or class-conditioned features [27, 34, 55]. Some methods instead deliberately learn domain-specific knowledge while leveraging domain-invariant information common to the source and target [5, 10]. In section 5.2 we show that adversarial training [16] complements our method but is not an adequate substitute for contact labels.

Deep Learning with Weak Labels: In cases where full labels are not available, approaches have been developed to still use partially or *weakly* labeled data. Prior work has

used semantic segmentation as a motivating task, where generating per-pixel labels requires significant time from human annotators [14]. Techniques have been developed to leverage faster annotations, including image-level labels [1, 11, 30] and point labels [3]. Most similar to our paper is work that leverages image-level labels and an adversarial loss to transfer segmentation models to new domains [41].

In contrast to weak labels applied by human annotators after data collection, our method prompts human behavior while data is being collected. People can often determine if an image shows a hand that is far from making contact or a hand that is holding a grasped object. In contrast, distinguishing between near contact, low force contact, and high force contact for specific regions of the hand is challenging even for experts.

3. Data Collection

We leverage the human ability to achieve contact and force objectives with their hand *at collection time*. For each data capture sequence, we prompt a participant to make contact with a surface using a specific combination of fingertips to achieve a target force level. We assign a contact label associated with the prompted finger combination and force level to all images in our dataset.

3.1. Collection Method

We collect two types of data: *fully labeled* data and *weakly labeled* data. For both types of sequences, we collect contact labels by prompting the subject with specific contact cues. For the fully labeled sequences, we additionally collect ground truth pressure labels using a high-resolution pressure sensing array [40].

As shown in Figure 3, a contact label W is represented

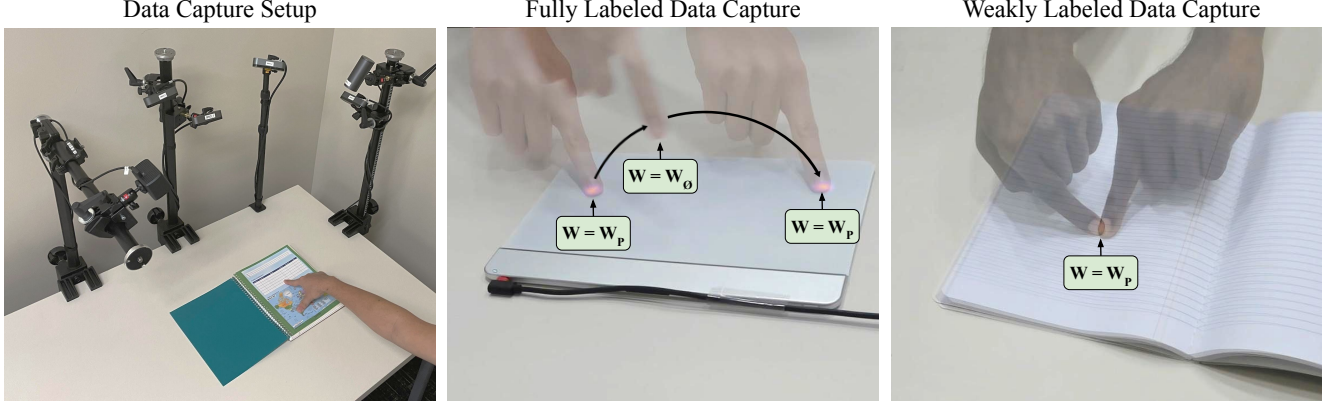


Figure 4. **Left:** Data capture setup in one of three environments. Camera angles were varied between each participant. **Center:** Data involving dynamic contact was collected for participants interacting with a high-resolution pressure sensor. Frames with measured pressure are given the prompted contact label W_P , and frames without measured pressure are given a no-contact label W_\emptyset . **Right:** Data involving static contact was collected for participants interacting with uninstrumented surfaces. All static contact frames are assigned the same contact label. Contact labels follow the format shown in Figure 3.

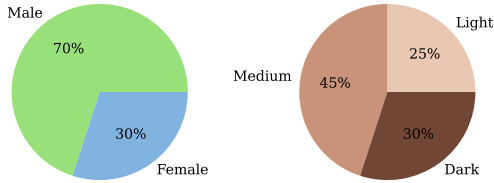


Figure 5. Participants with a range of genders and skin tones were recruited for our study.

as a vector with 6 elements. The first 5 elements indicate the presence or lack of contact at each of the 5 fingertips. The sixth element indicates if the participant was prompted to exert a low, high, or unspecified force.

We represent a contact label $W \in \mathbb{Z}^6$ as follows:

$$w_i|_{0 \leq i \leq 4} \in \{0, 1\} \equiv \{\text{no contact}, \text{contact}\}$$

$$w_i|_{i=5} \in \{-1, 0, 1\} \equiv \{\text{unspecified}, \text{low}, \text{high force}\}$$

For fully labeled data collection, both pressure labels and contact labels are collected. The participant is prompted to press a specified set of fingers onto a pressure sensor with a given force level. Data recording begins with the hand out of frame, then the participant presses and releases their hand multiple times on the sensor. The collection captures the onset and termination of contact as the participant performs multiple touches (Figure 4 middle). Frames where contact is detected by the pressure sensor are assigned the contact label associated with the prompted pressing action. Frames where no measurable force is detected are assigned a “no-contact” label.

For weakly labeled data collection, only contact labels

are collected. We use uninstrumented objects and ask participants to make contact for the entire duration of the recording. Before capture, the participant first makes contact with specified fingers on a surface. Once recording starts, the participant maintains contact for the duration of the video while varying the pose of the hand (Figure 4 right). We rely on the participant to faithfully execute the prompted action.

During all data capture sequences, the participant is prompted with a specific action, for example, “press ring finger, low force”. The participant performs the requested action while data is collected. This action corresponds with a contact label (Figure 3) used for training.

3.2. Data Splits

Our training data comes from fourteen participants. Our testing data comes from six participants who are not present in the training data. The details follow:

- **Fully labeled training set:** Participants touched a solid-colored overlay (black, white, gray, or blue) placed on top of a pressure-sensing array.
- **Weakly labeled training set:** Participants touched ten surfaces, including a textbook, a notebook, and glass.
- **Fully labeled test set:** Participants touched an overlay (mirrored, granite, wood, or text) placed on top of a pressure-sensing array. The granite and wood overlays are not present in either training set.
- **Weakly labeled test set:** Participants touched glass, foam, a wall, a football, a book, and a mirror. The book is not present in either training set. The other objects are present in the weakly labeled training set.

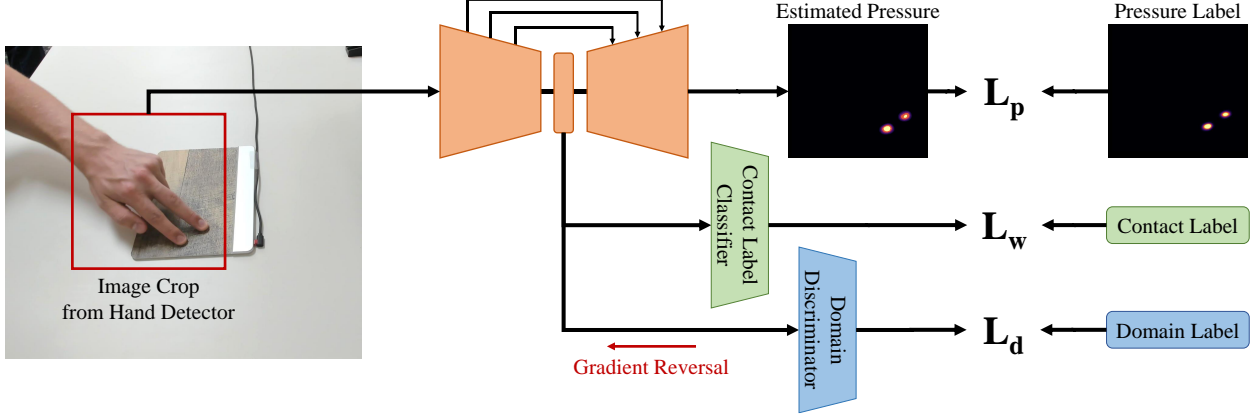


Figure 6. ContactLabelNet architecture. An RGB input image is first cropped using the bounding box from an off-the-shelf hand detector. The cropped image is passed into an encoder-decoder network to estimate pressure for each pixel in the input image. Two classification heads are attached to the bottleneck of the network; one is trained to estimate the contact label, and the other uses an adversarial loss to discriminate between the source and target domains.

We simultaneously collected video with up to six consumer-grade webcams manufactured by Logitech, Dell, and Elgato at 1080p resolution. We conducted data collection in three environments with different lighting conditions. We used a Sensel Morph [40] pressure sensing array. All data was synchronized and collected at 30 FPS. For each participant, we collected data with two objects – one object per hand.

For all data collection procedures, we prompted participants to press one of 8 combinations of fingertips onto a surface. For each combination, we prompted the participant to apply low force, high force, or slide with unspecified force. Additionally, for each combination, we prompted participants to make “no contact” by hovering the specified fingertips just above the surface.

3.3. Ethics

Approval to conduct this study was obtained from a university Institutional Review Board (IRB). We recruited a diverse set of 20 participants (Figure 5). All participants gave informed consent and were compensated for their time. We measured skin tone with a Pantone X-Rite RM200 spectrophotometer, and participants self-reported gender.

4. Network Architecture

We create a network (Figure 6) to take a single RGB image, I , as input and then output a pressure image, $\hat{P} = f(I)$. For fully-labeled data, each RGB image is paired with a ground-truth pressure image obtained by projecting the output of a pressure sensing array into the image using a homography transform. The output pressure \hat{P} is in *image space*, such that the input and output images are the same shape and can be superimposed (Figure 7).

4.1. Pressure Estimation

To estimate pressure, ContactLabelNet uses a binned representation and performs a classification across bins. The pressure range is split into $N_B = 9$ bins divided across the pressure range, including one zero bin. Pressure estimation uses a *structure-aware cross-entropy loss* L_p [39, 50]. Intuitively, the structure-aware loss penalizes large errors more than small errors. For each pressure pixel over the image x, y , the loss is computed over all bin indices $b \in B$ using the ground truth index k_b and the estimated probability for each bin $\rho_{x,y}(b)$.

$$L_p = - \sum_{x,y} \sum_b e^{-|b-k_b|} \log(\rho_{x,y}(b)) \quad (1)$$

L_p is only computed when fully labeled data is available.

4.2. Contact Label Estimation

In addition to estimating a pressure image, ContactLabelNet performs the auxiliary task of estimating the contact label \hat{W} . The contact label classifier predicts \hat{W} using the features F at the network bottleneck (Figure 6). The addition of the contact label classifier ensures that the features generated by the encoder are discriminative to the set of fingers in contact and the force level. The classifier pools features and uses a 2-layer MLP to estimate the contact label collected in Section 3.1. This classifier is trained with a binary cross-entropy loss L_w . However, to account for cases when the force level is unspecified, loss is not calculated for negative values.

4.3. Adversarial Domain Adaptation

In addition to regularizing the network by applying the contact label loss, we apply an additional feature alignment

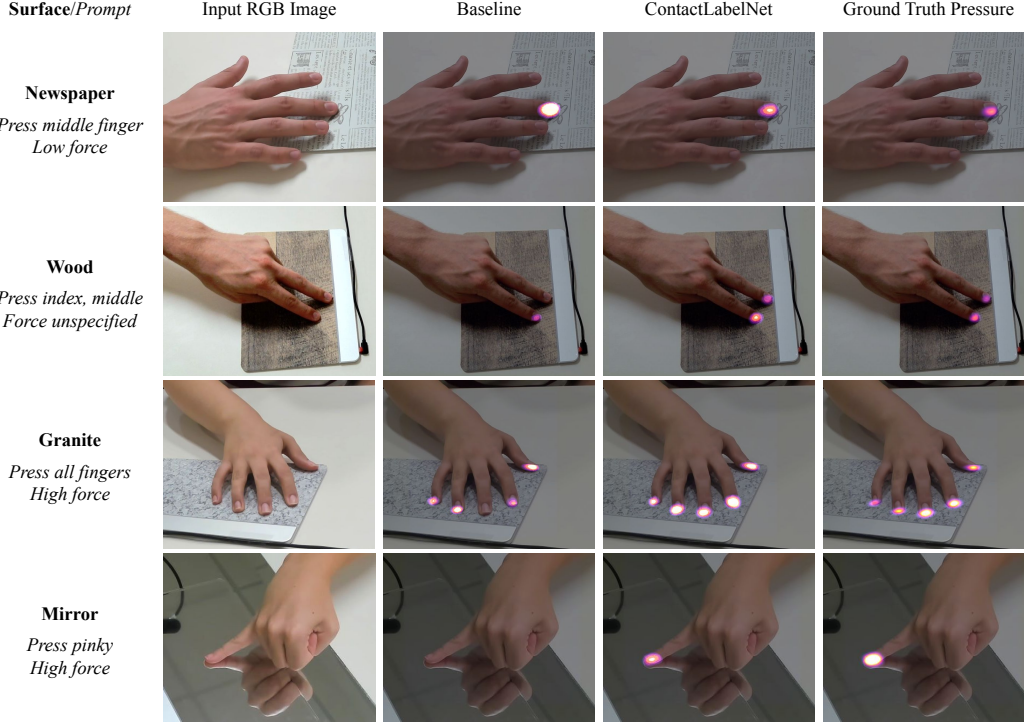


Figure 7. Results on the fully labeled test set. The baseline column is ContactLabelNet trained without either the domain loss or contact label loss. The full ContactLabelNet is shown to perform well on unseen surfaces, and benefits significantly from both losses.

loss. This loss attempts to minimize the difference between the distributions of features generated from the source and target domains, following prior work in domain adaptation [16]. This loss is *unsupervised*, as it does not leverage contact label information.

We implement this feature-alignment loss using a domain discriminator D , which operates on features from the network bottleneck with a similar architecture to the weak label classifier. The discriminator attempts to identify if the image is from the fully labeled or weakly labeled domain. When backpropagating, gradients are reversed upstream of the domain discriminator [16]. For image features from the source domain F_s and target domain F_t , the domain loss function L_d is:

$$L_d = -\log(D(F_s)) - \log(1 - D(F_t)) \quad (2)$$

4.4. Training Details

Due to the wide angle of the captured images, ContactLabelNet operates on crops of the hand. We use Google MediaPipe [35] to produce hand detections, and use these bounding boxes to crop the image. Images are resized to 448x448 pixels.

ContactLabelNet is trained end-to-end using the following loss function:

$$L = L_p + \lambda_1 L_w + \lambda_2 L_d \quad (3)$$

ContactLabelNet uses an SE-ResNeXt-50 encoder [20, 23, 54] and an FPN decoder [32, 56]. ContactLabelNet was trained for 300k iterations, and optimized with the Adam optimizer [29]. We choose $\lambda_1 = 0.01$ and $\lambda_2 = 0.001$. Each batch contains an equal number of weakly and fully labeled samples.

5. Evaluation

We consider two types of evaluations, *contact* and *pressure* evaluations. Contact is a binary quantity indicating if the hand and object are touching, while pressure is a scalar indicating the magnitude of force. A binary contact image \hat{C} is generated by thresholding pressure \hat{P} at $P_{th} = 1 \text{ kPa}$. These evaluations are inspired from prior work [17].

- **Contact Accuracy:** the estimated contact image \hat{C} is used to determine if *any* contact is estimated. Accuracy is calculated by counting the percentage of video frames for which \hat{C} corresponds with the contact label.
- **Contact IoU:** intersection-over-union (IoU) is computed between the ground truth contact image C and estimated contact image \hat{C} . This is the upper bound on Volumetric IoU.
- **Volumetric IoU:** as an extension of Contact IoU that considers the *magnitude* of pressure, 2D pressure im-

Method	Fully-Labeled Test Set			Weakly-Labeled Test Set
	Contact Acc.	Contact IoU	Volumetric IoU	Contact Acc.
Zero Guesser	49.0%	0.0%	0.0%	23.4%
PressureVisionNet [17] (original)	52.8%	1.5%	1.2%	40.8%
PressureVisionNet [17] (retrained)	70.2%	16.3%	13.1%	45.6%
ContactLabelNet (ours)	90.4%	44.3%	30.6%	87.4%

Table 1. Performance compared to PressureVisionNet baseline [17]. Our method outperforms the baselines by a large margin.

ages are viewed as 3D pressure volumes, where the height of the volume is proportional to the magnitude of pressure $P_{x,y}$. Intersection-over-union is computed using these volumes.

$$IoU_{vol} = \frac{\sum_{x,y} \min(P_{x,y}, \hat{P}_{x,y})}{\sum_{x,y} \max(P_{x,y}, \hat{P}_{x,y})} \quad (4)$$

For the same reasons that collecting fully-labeled training data on diverse surfaces is difficult, collecting fully-labeled testing data also presents challenges. We evaluate both the *fully labeled* and *weakly labeled* test sets. However, due to the lack of pressure measurements in the weakly labeled test set, only contact accuracy is computed.

5.1. Performance Compared to Baselines

We compare our method against two baselines:

- **Zero Guesser:** The zero guesser always outputs a zero pressure image, and provides a simple baseline for Contact Accuracy due to the large number of frames with no contact.
- **PressureVisionNet:** The network from [17], using either the original weights or retrained on our fully-labelled data. This method does not use contact labels.

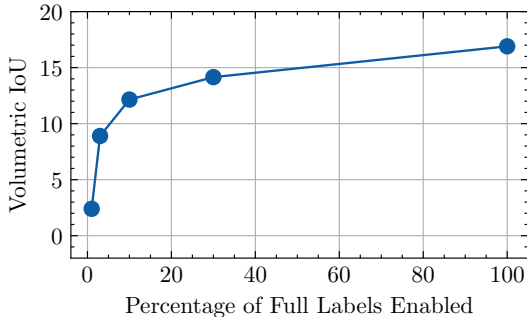


Figure 8. To quantify the value of weakly-labeled images versus fully-labeled images, we remove a percentage of the pressure labels, but leave all images with contact labels. Volumetric IoU is evaluated on the fully-labeled test set.

Table 1 shows the performance of baselines compared to ContactLabelNet on the test sets. ContactLabelNet significantly outperforms prior work, improving on all metrics. Examples of pressure estimation on the fully-labeled test set are shown in Figure 7, and examples from the weakly-labeled test set are shown in Figure 9.

ContactLabelNet estimates fingertip pressure on diverse surfaces, including textured, deformable, and curved surfaces. Notably, *none* of the testing surfaces were included in the fully-labeled training set. Our method adapts to these surfaces using only weakly-labeled training data. Additionally, two surface textures are completely unseen during training (wood and granite), indicating that our approach can successfully generalize to novel surfaces.

When performance on the test set is separated by object type (full table in supplementary material), we observe that our approach performs most poorly on mirrors and glass, achieving a contact accuracy of 72% and 75%, respectively. We suspect that this is due to significant appearance differences from other surfaces in the training set (Figure 9), including a lack of shadows. As shown in prior work [17], performance is sensitive to shadows. We also observe that ContactLabelNet reports no contact for occluded fingertips.

5.2. Ablating Domain Loss and Contact Label Loss

Table 2 illustrates how the domain loss and contact label loss impact ContactLabelNet’s performance. The table shows results from ablating the two auxiliary losses. We trained ContactLabelNet with each combination of the domain loss and contact label loss enabled or disabled. Both losses significantly contribute to performance. Compared to the baseline with neither loss enabled, the domain loss improves the relative volumetric IoU by +27%, the contact label loss improves the metric by +51%, and both combined improve the metric by +69%.

The performance improvement with contact labels demonstrates the value of weak supervision. The difficulty of weakly labeled data collection is comparable to that of unlabeled data collection, yet it provides a significant increase in performance over unlabeled data. Weakly-labeled data improves performance for diverse surfaces that can be difficult to instrument.



Figure 9. Results on the surfaces in weakly labeled test set, *none* of which are included in the fully labeled training set. ContactLabelNet produces qualitatively accurate results on highly-textured, curved, and compliant surfaces, but may not perform as well on surfaces that are transparent and reflective (see bottom row). Note that we did not obtain full pressure labels for these objects.

Domain Loss	Contact Label Loss	Fully-Labeled Test Set			Weakly-Labeled Test Set
		Contact Acc.	Contact IoU	Volumetric IoU	Contact Acc.
		73.6%	21.5%	18.1%	60.0%
✓		82.6%	32.5%	23.1%	64.8%
	✓	88.8%	40.2%	27.3%	84.0%
✓	✓	90.4%	44.3%	30.6%	87.4%

Table 2. We evaluate ContactLabelNet when the network losses are ablated. The domain loss and the contact label loss enable leveraging weakly-labeled training data, and both improve performance significantly.

5.3. Performance with Full versus Weak Labels

We perform an additional evaluation to quantify the value of weakly-labeled images versus fully-labeled images. We train the network on *only the fully-labeled training set*, and artificially remove the full labels, providing the network with 1% to 100% fully-labeled data. As shown in Figure 8, performance quickly improves as the percentage of fully-labeled data is increased, indicating that weakly-labeled data may be a strong substitute for fully labeled data.

6. Conclusion

Training deep models to visually estimate the pressure applied by fingertips relies on ground-truth pressure measurements that are difficult to obtain. We presented ContactLabelNet which uses more easily obtained contact labels collected by prompting participants to achieve specific types of contact. Leveraging this weakly supervised data is shown to improve pressure estimation on diverse surfaces and outperforms prior methods.

References

- [1] Jiwoon Ahn and Suha Kwak. Learning pixel-level semantic affinity with image-level supervision for weakly supervised semantic segmentation. In *Proceedings of the IEEE conference on computer vision and pattern recognition*, pages 4981–4990, 2018. 3
- [2] Karan Ahuja, Paul Strelci, and Christian Holz. TouchPose: Hand pose prediction, depth estimation, and touch classification from capacitive images. In *The 34th Annual ACM Symposium on User Interface Software and Technology*, pages 997–1009, 2021. 2
- [3] Amy Bearman, Olga Russakovsky, Vittorio Ferrari, and Li Fei-Fei. What’s the point: Semantic segmentation with point supervision. In *European conference on computer vision*, pages 549–565. Springer, 2016. 3
- [4] Raunaq Bhirangi, Tess Hellebrekers, Carmel Majidi, and Abhinav Gupta. Reskin: versatile, replaceable, lasting tactile skins. *Conference on Robot Learning (CoRL)*, 2021. 2
- [5] Konstantinos Bousmalis, George Trigeorgis, Nathan Silberman, Dilip Krishnan, and Dumitru Erhan. Domain separation networks. *Advances in neural information processing systems*, 29, 2016. 3
- [6] Samarth Brahmabhatt, Cusuh Ham, Charles C. Kemp, and James Hays. ContactDB: Analyzing and predicting grasp contact via thermal imaging. In *CVPR*, June 2019. 2
- [7] Samarth Brahmabhatt, Chengcheng Tang, Christopher D. Twigg, Charles C. Kemp, and James Hays. ContactPose: A dataset of grasps with object contact and hand pose. In *ECCV*, August 2020. 2
- [8] Samarth Manoj Brahmabhatt. *Grasp contact between hand and object: Capture, analysis, and applications*. PhD thesis, Georgia Institute of Technology, 2020. 2
- [9] Gereon H Büscher, Risto Kõiva, Carsten Schürmann, Robert Haschke, and Helge J Ritter. Flexible and stretchable fabric-based tactile sensor. *Robotics and Autonomous Systems*, 63:244–252, 2015. 2
- [10] Woong-Gi Chang, Tackgeun You, Seonguk Seo, Suha Kwak, and Bohyung Han. Domain-specific batch normalization for unsupervised domain adaptation. In *Proceedings of the IEEE/CVF conference on Computer Vision and Pattern Recognition*, pages 7354–7362, 2019. 3
- [11] Yu-Ting Chang, Qiaosong Wang, Wei-Chih Hung, Robinson Piramuthu, Yi-Hsuan Tsai, and Ming-Hsuan Yang. Weakly-supervised semantic segmentation via sub-category exploration. In *Proceedings of the IEEE/CVF Conference on Computer Vision and Pattern Recognition*, pages 8991–9000, 2020. 3
- [12] Nutan Chen, Göran Westling, Benoni B Edin, and Patrick van der Smagt. Estimating fingertip forces, torques, and local curvatures from fingernail images. *Robotica*, 38(7):1242–1262, 2020. 3
- [13] Frederick Choi, Sven Mayer, and Chris Harrison. 3d hand pose estimation on conventional capacitive touchscreens. In *Proceedings of the 23rd International Conference on Mobile Human-Computer Interaction*, MobileHCI ’21, New York, NY, USA, 2021. Association for Computing Machinery. 2
- [14] Marius Cordts, Mohamed Omran, Sebastian Ramos, Timo Rehfeld, Markus Enzweiler, Rodrigo Benenson, Uwe Franke, Stefan Roth, and Bernt Schiele. The cityscapes dataset for semantic urban scene understanding. In *Proceedings of the IEEE conference on computer vision and pattern recognition*, pages 3213–3223, 2016. 3
- [15] Kiana Ehsani, Shubham Tulsiani, Saurabh Gupta, Ali Farhadi, and Abhinav Gupta. Use the force, Luke! Learning to predict physical forces by simulating effects. In *CVPR*, pages 224–233, 2020. 2
- [16] Yaroslav Ganin, Evgeniya Ustinova, Hana Ajakan, Pascal Germain, Hugo Larochelle, François Laviolette, Mario Marchand, and Victor Lempitsky. Domain-adversarial training of neural networks. *The journal of machine learning research*, 17(1):2096–2030, 2016. 3, 6
- [17] Patrick Grady, Chengcheng Tang, Samarth Brahmabhatt, Christopher D. Twigg, Chengde Wan, James Hays, and Charles C. Kemp. PressureVision: estimating hand pressure from a single RGB image. *European Conference on Computer Vision (ECCV)*, 2022. 1, 3, 6, 7
- [18] Patrick Grady, Chengcheng Tang, Christopher D. Twigg, Minh Vo, Samarth Brahmabhatt, and Charles C. Kemp. ContactOpt: Optimizing contact to improve grasps. In *CVPR*, pages 1471–1481, 2021. 3
- [19] Anhong Guo, Robert Xiao, and Chris Harrison. Capauth: Identifying and differentiating user handprints on commodity capacitive touchscreens. In *Proceedings of the 2015 International Conference on Interactive Tabletops & Surfaces*, pages 59–62, 2015. 2
- [20] Kaiming He, Xiangyu Zhang, Shaoqing Ren, and Jian Sun. Deep residual learning for image recognition. In *CVPR*, pages 770–778, 2016. 6
- [21] Helen H Hu, Amy A Gooch, Sarah H Creem-Regehr, and William B Thompson. Visual cues for perceiving distances from objects to surfaces. *Presence: Teleoperators & Virtual Environments*, 11(6):652–664, 2002. 3
- [22] Helen H Hu, Amy A Gooch, William B Thompson, Brian E Smits, John J Rieser, and Peter Shirley. Visual cues for imminent object contact in realistic virtual environments. In *Proceedings Visualization 2000.*, pages 179–185. IEEE, 2000. 3
- [23] Jie Hu, Li Shen, and Gang Sun. Squeeze-and-excitation networks. In *CVPR*, pages 7132–7141, 2018. 6
- [24] Geoffrey S. Hubona, Philip N. Wheeler, Gregory W. Shirah, and Matthew Brandt. The relative contributions of stereo, lighting, and background scenes in promoting 3d depth visualization. *ACM Transactions on Computer Human Interaction*, 6(3):214–242, 1999. 3
- [25] Wonjun Hwang and Soo-Chul Lim. Inferring interaction force from visual information without using physical force sensors. *Sensors*, 17(11):2455, 2017. 3
- [26] Roland S. Johansson and J. Randall Flanagan. Coding and use of tactile signals from the fingertips in object manipulation tasks. *Nat Rev Neurosci*, 10:345–359, 2009. 1
- [27] Guoliang Kang, Lu Jiang, Yi Yang, and Alexander G Hauptmann. Contrastive adaptation network for unsupervised domain adaptation. In *Proceedings of the IEEE/CVF Confer-*

- ence on Computer Vision and Pattern Recognition, pages 4893–4902, 2019. 3
- [28] Hong-Ki Kim, Seunggun Lee, and Kwang-Seok Yun. Capacitive tactile sensor array for touch screen application. *Sensors and Actuators A: Physical*, 165(1):2–7, 2011. 2
- [29] Diederik P. Kingma and Jimmy Ba. Adam: A method for stochastic optimization. In *3rd International Conference on Learning Representations (ICLR)*, 2015. 6
- [30] Alexander Kolesnikov and Christoph H Lampert. Seed, expand and constrain: Three principles for weakly-supervised image segmentation. In *European conference on computer vision*, pages 695–711. Springer, 2016. 3
- [31] Zongmian Li, Jirí Sedlár, Justin Carpentier, Ivan Laptev, Nicolas Mansard, and Josef Sivic. Estimating 3d motion and forces of person-object interactions from monocular video. In *CVPR*, pages 8640–8649, 2019. 2
- [32] Tsung-Yi Lin, Piotr Dollár, Ross Girshick, Kaiming He, Bharath Hariharan, and Serge Belongie. Feature pyramid networks for object detection. In *CVPR*, pages 2117–2125, 2017. 6
- [33] Mingsheng Long, Yue Cao, Jianmin Wang, and Michael Jordan. Learning transferable features with deep adaptation networks. In *International conference on machine learning*, pages 97–105. PMLR, 2015. 3
- [34] Mingsheng Long, Zhangjie Cao, Jianmin Wang, and Michael I Jordan. Conditional adversarial domain adaptation. *Advances in neural information processing systems*, 31, 2018. 3
- [35] Camillo Lugaresi, Jiuqiang Tang, Hadon Nash, Chris McClanahan, Esha Uboweja, Michael Hays, Fan Zhang, Chuoling Chang, Ming Yong, Juhyun Lee, Wan-Teh Chang, Wei Hua, Manfred Georg, and Matthias Grundmann. Mediapipe: A framework for perceiving and processing reality. In *Third Workshop on Computer Vision for AR/VR at IEEE Computer Vision and Pattern Recognition (CVPR) 2019*, 2019. 6
- [36] Yiyue Luo, Yunzhu Li, Pratyusha Sharma, Wan Shou, Kui Wu, Michael Foshey, Beichen Li, Tomás Palacios, Antonio Torralba, and Wojciech Matusik. Learning human-environment interactions using conformal tactile textiles. *Nature Electronics*, 4(3):193–201, 2021. 2
- [37] Stephen A Mascaro and H Harry Asada. Photoplethysmograph fingernail sensors for measuring finger forces without haptic obstruction. *IEEE Transactions on Robotics and Automation*, 17(5):698–708, 2001. 3
- [38] Stephen A. Mascaro and H. Harry Asada. Measurement of finger posture and three-axis fingertip touch force using fingernail sensors. *IEEE Transactions on Robotics and Automation*, 20(1):26–35, 2004. 3
- [39] Francisco Massa, Renaud Marlet, and Mathieu Aubry. Crafting a multi-task CNN for viewpoint estimation. *BVMC*, 2016. 5
- [40] Morph. Sensel Morph haptic sensing tablet. www.sensel.com/pages/the-sensel-morph, Last accessed on 2020-02-25. 2, 3, 5
- [41] Sujoy Paul, Yi-Hsuan Tsai, Samuel Schuster, Amit K Roy-Chowdhury, and Manmohan Chandraker. Domain adaptive semantic segmentation using weak labels. In *European conference on computer vision*, pages 571–587. Springer, 2020. 2, 3
- [42] Tu-Hoa Pham, Abderrahmane Kheddar, Ammar Qammar, and Antonis A. Argyros. Towards force sensing from vision: Observing hand-object interactions to infer manipulation forces. In *CVPR*, pages 2810–2819, 2015. 2
- [43] Tu-Hoa Pham, Nikolaos Kyriazis, Antonis A. Argyros, and Abderrahmane Kheddar. Hand-object contact force estimation from markerless visual tracking. *IEEE Transactions on Pattern Analysis and Machine Intelligence*, 40(12):2883–2896, 2017. 2
- [44] Pressure Profile Systems. PPS TactileGlove. 2
- [45] M Reinvee, K Jansen, et al. Utilisation of tactile sensors in ergonomic assessment of hand-handle interface: a review. *Agron. Res*, 12(3):907–914, 2014. 1
- [46] George Woolliscroft Rhead. *The principles of design: A text book for teacher, students and craftsmen*. BT Batsford, 1905. 3
- [47] Grégory Rogez, James S Supancic, and Deva Ramanan. Understanding everyday hands in action from RGB-D images. In *ICCV*, pages 3889–3897, 2015. 2
- [48] Jung-Sim Roh, Yotam Mann, Adrian Freed, David Wessel, UC Berkeley, A Freed, A Street, and D Wessel. Robust and reliable fabric, piezoresistive multitouch sensing surfaces for musical controllers. In *NIME*, pages 393–398, 2011. 1
- [49] Yi Chang Shih, Abe Davis, Samuel W. Hasinoff, Frédo Durand, and William T. Freeman. Laser speckle photography for surface tampering detection. In *2012 IEEE Conference on Computer Vision and Pattern Recognition*, pages 33–40, 2012. 2
- [50] Hao Su, Charles R Qi, Yangyan Li, and Leonidas J Guibas. Render for CNN: Viewpoint estimation in images using CNNs trained with rendered 3d model views. In *Proceedings of the IEEE international conference on computer vision*, pages 2686–2694, 2015. 5
- [51] Subramanian Sundaram, Petr Kellnhofer, Yunzhu Li, Jun-Yan Zhu, Antonio Torralba, and Wojciech Matusik. Learning the signatures of the human grasp using a scalable tactile glove. *Nature*, 569(7758):698–702, 2019. 1, 2
- [52] Tekscan. Pressure mapping, force measurement and tactile sensors. www.tekscan.com/products-solutions/sensorsLast, Last accessed on 2020-02-25. 2
- [53] Eric Tzeng, Judy Hoffman, Ning Zhang, Kate Saenko, and Trevor Darrell. Deep domain confusion: Maximizing for domain invariance. *arXiv preprint arXiv:1412.3474*, 2014. 3
- [54] Saining Xie, Ross B. Girshick, Piotr Dollár, Zhuowen Tu, and Kaiming He. Aggregated residual transformations for deep neural networks. In *CVPR*, pages 5987–5995, 2017. 6
- [55] Shaoan Xie, Zibin Zheng, Liang Chen, and Chuan Chen. Learning semantic representations for unsupervised domain adaptation. In *International conference on machine learning*, pages 5423–5432. PMLR, 2018. 3
- [56] Pavel Yakubovskiy. Segmentation models Pytorch, 2020. 6